Conclusion

An analysis of the UV photoelectron spectra of gaseous mixtures of $(CH_3)_2S$ and HF has indicated the presence of the trimeric intermolecular complex $(CH_3)_2S\cdot(HF)_2$. This is identified by its first PE band, associated with the localized nonbonding sulfur 3p electrons, which is 0.8 eV higher than that of the dimer $(CH_3)_2S\cdot HF$ and 1.6 eV above that of the $(CH_3)_2S$ monomer. A comparison of these IE shifts with typical hydrogen bond energies suggests that the complex ions produced by UV ionization are quite unstable.

Acknowledgment. This work was supported by the Australian Research Grants Scheme.

Registry No. $(CH_3)_2\cdot HF$, 87261-56-1; $(CH_3)_2S\cdot(HF)_2$, 87261-57-2.

EPR and ODMR Studies of the Lowest Excited Triplet States of Two Tautomers of Indazole in a Benzoic Acid Host Crystal

Masayo Noda[†,‡] and Noboru Hirota*[†]

Contribution from the Department of Chemistry, Faculty of Science, Kyoto University, Kyoto 606, Japan, and Tokai Women's College, Kagamigahara City, Gifu 504, Japan.
Received February 1, 1983

Abstract: It is shown that, in a benzoic acid host, indazole in the T_1 state exists in two tautomeric forms (abbreviated as 1H and 2H). The properties of the T_1 states of both tautomers are investigated by means of EPR and zero-field ODMR techniques. The T_1 state of 1H is located 23 590 cm^{-1} above the ground state while that of 2H is 20 903 cm^{-1}. Zero-field splittings of two tautomers are $D = 0.1077$ cm^{-1} and $|E| = 0.0293$ cm^{-1} for 1H and $D = 0.0983$ cm^{-1} and $|E| = 0.0120$ cm^{-1} for 2H, respectively. The phosphorescence decay takes place predominantly from the middle sublevel in both tautomers, but the decay rate constant of 2H is about 5 times larger than that of 1H, which is likely due to the larger nonradiative decay rate constant. From the angular dependence of the EPR signals, the orientations of the two tautomers in benzoic acid are determined. Spin distributions of the two tautomers are estimated from the analysis of the hyperfine splittings and are compared with the result of π-electron UHF calculations. Good agreement was obtained in the case of 2H. The low-field EPR signals exhibit hyperfine anomalies due to forbidden transitions.

The lowest excited triplet (T_1) states of purine, benzimidazole, and indole have received considerable attention because of their possible importance in photobiological processes.[1-11] Indazole is interesting as a member of this series of molecules but also from viewpoints of tautomerism and photochemistry.

Indazole has two tautomeric forms (1*H*- and 2*H*-indazole are hereafter abbreviated as 1H and 2H, respectively), as shown in Figure 1. The question whether indazole can exist in two different forms in nature has attracted much interest. Rousseau and Lindwall[12] compared the UV absorption spectrum of indazole with those of 1-methyl- and 2-methylindazole and concluded that 2H does not exist in water. Buu-Hoi et al.[13] and Black et al.[14] studied the NMR spectra in acetone and chloroform and also concluded that the 1H form is predominant. An ^{14}N NMR investigation by Witanowski et al.[15] showed that only the 1H form exists in acetone. An X-ray study of the indazole crystal[16] shows that indazole exists in the 1H form in the crystal. Therefore, so far there has been no experimental evidence that indazole exists in the 2H form. It seems interesting to examine the possibility that both forms of tautomers might exist in the T_1 state in a favorable environment.

The photochemistry of indazole has been investigated by several workers.[17-20] The transposition of the nitrogen atom to produce benzimidazole and the isomerization into *o*-aminobenzonitrile are known to take place photochemically. The T_1 state may play an important role in these reactions.

In the present work we have studied the T_1 state of indazole in the mixed single crystal of benzoic acid (abbreviated as BAC) by means of EPR and zero-field ODMR techniques at liquid helium temperatures. The BAC host is particularly suited to the present study because indazole dissolves into BAC by forming hydrogen bonds with BAC. We have found that in the T_1 states both 1H and 2H exist in the BAC host and studied the properties of the T_1 states of both tautomers in detail. Interestingly, the magnetic and decay properties of these tautomers are rather

[†] Kyoto University.
[‡] Tokai Women's College.

(1) S. P. McGlynn, T. Azumi, and M. Kinoshita, "Molecular Spectroscopy of the Triplet State", Prentice-Hall, Englewood Cliffs, NJ, 1969.
(2) R. S. Becker, "Theory and Interpretation of Phosphorescence and Fluorescence", Wiley, New York, 1969.
(3) A. B. Zahlan, Ed. "The Triplet State", Cambridge University Press, New York, 1967.
(4) B. J. Cohen and L. Goodman, *J. Am. Chem. Soc.*, **87**, 5787 (1965).
(5) J. Drobnik and L. Augenstein, *Photochem. Photobiol.*, **5**, 13 (1966).
(6) M. J. Robey and I. G. Ross, *Photochem. Photobiol.*, **21**, 365 (1975).
(7) J. W. Longworth, R. O. Rahn, and R. G. Shulman, *J. Chem. Phys.*, **45**, 2930 (1966).
(8) J. J. Smith, *Photochem. Photobiol.*, **23**, 365 (1976).
(9) J. J. Smith, *Spectrochim. Acta, Part A* **33A**, 135 (1977).
(10) G. Moller and A. M. Nishimura, *J. Phys. Chem.*, **81**, 147 (1977).
(11) P. Svejda, R. R. Anderson, and A. H. Maki, *J. Am. Chem. Soc.*, **100**, 7131 (1978).
(12) V. Rousseau and G. H. Lindwall, *J. Am. Chem. Soc.*, **72**, 3047 (1950).
(13) N. P. Buu-Hoi, J. Foeffinger, and P. Jacquignon, *Bull. Soc. Chim. Fr.*, 2019 (1964).
(14) P. J. Black and M. L. Heffernan, *Aust. J. Chem.*, **16**, 1051 (1963).
(15) M. Witanowski, L. Stefaniak, H. Januszewski, and Z. Grabowski, *Tetrahedron*, **28**, 637 (1972).
(16) A. Escande and J. Lapasset, *Acta Crystallogr.*, **B30**, 2009 (1974).
(17) J. P. Ferris, K. V. Prabhu, and R. L. Strong, *J. Am. Chem. Soc.*, **97**, 2385 (1975).
(18) H. Tiefenthaler, W. Dörscheln, H. Göth, and H. Schmidt, *Helv. Chim. Acta*, **50**, 2244 (1967).
(19) H. Tiefenthaler, W. Dorscheln, H. Goth, and H. Schmidt, *Tetrahedron Lett.*, 2999 (1964).
(20) W. Heinzelmann, M. Marky, and P. Gilgen, *Helv. Chim. Acta* **59**, 1512 (1976).

0002-7863/83/1505-6790$01.50/0 © 1983 American Chemical Society

Table I. Energy and Zero-Field Splittings of the Lowest Triplet States of Several Indazoles[a]

guest	host	triplet energy, cm^{-1}	D, cm^{-1}	$\|E\|$, cm^{-1}	ODMR signals, GHz		
					XY	YZ	ZX
1*H*-indazole	BAC	23 590	0.1077	0.0293	1.76	2.35	*b*
2*H*-indazole	BAC	20 903	0.0983	0.0120	0.72	2.59	*b*
1*H*-indazole	DBB	23 753[c]	0.1100	0.0317	1.90	2.35	4.25
1-methylindazole	DBB	23 167	0.1065	0.0315	1.89	2.25	*b*
2-methylindazole	DBB	20 580	0.0960	0.0107	0.64	2.56	3.18
1-methylindazole[d]	ethanol–methanol	23 343	0.102	0.031			
2-methylindazole[d]	ethanol–methanol	21 427	0.092	0.014			

[a] Estimated error is 5 cm^{-1} for energy and 0.005 cm^{-1} for zero-field splitting. [b] Not observed. [c] Reference 30. [d] Reference 17.

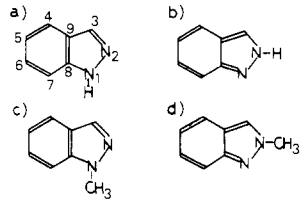

Figure 1. Molecular structures and the numbering systems for (a) 1*H*-indazole, (b) 2*H*-indazole, (c) 1-methylindazole, and (d) 2-methylindazole.

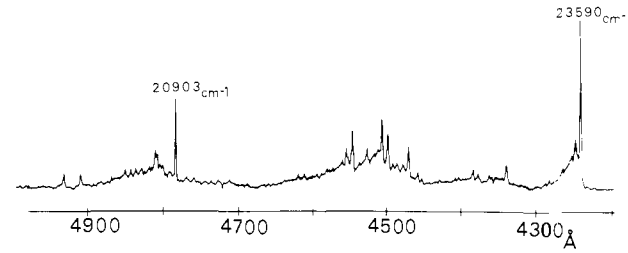

Figure 2. Phosphorescence spectrum of indazole in the mixed crystal of BAC at 4.2 K.

different. Here, we discuss the sublevel decay properties, orientations of indazole in the BAC host, zero-field splittings (zfs), hyperfine splittings (hfs), hyperfine anomalies, and the spin distributions in the two tautomers.

Experimental Section

A. Sample Preparation. Single crystals of BAC and 1,4-dibromobenzene (DBB) containing small amounts of indazole were grown by the standard Bridgman method. BAC and DBB (Wako) were zone refined extensively prior to use. Indazole (Tokyokasei) was purified by repeated recrystallization from water and vacuum sublimation. 1-Methylindazole and 2-methylindazole were synthesized according to the procedures given by Auwers[21] and Schad,[22] respectively.

B. ODMR Measurements. Phosphorescence spectra were taken with a Spex 1704 spectrometer at 4.2 K. The zfs and decay rate constants were determined by the standard ODMR and microwave-induced delayed phosphorescence (MIDP) methods made at 1.5 K with the setup and procedures described previously.[23-27]

C. EPR Measurements. EPR measurements were made at 4.2 K with a JEOL JES-FE3X spectrometer and a finger tip cryostat. The experimental procedures are essentially the same as those described in a previous paper.[28] The crystal was mounted on a wedge so that the applied field rotated within the molecular plane of BAC by rotating the sample holder. BAC crystal is monoclinic ($P2_1/c$),[29] with four molecules per unit cell, but two pairs form a dimer unit connected by hydrogen bonds. Therefore two different angular dependences of the EPR signals are expected for the guest molecules which replace the host molecules by substitution. The crystal cleaves in the *ab* plane, and the directions of the *a* and *b* axes are identified by conoscopic observation. As discussed in the previous paper, there are four possible ways of mounting the crystal when the mounting is made by conoscopic observation only. However, two of them give identical EPR spectra because of the crystal structure of BAC; thus the probability of obtaining the right mounting is $^1/_2$.

Results and Discussion

A. Presence of Indazole Tautomers. The phosphorescence spectrum of indazole in BAC at 4.2 K is shown in Figure 2. The 0–0 band of the phosphorescence spectrum is located at 23 590 cm^{-1}, which is close to 23 753 cm^{-1} found in the DBB host[30] (Table I). At this band two ODMR signals were observed at 1.76 and 2.35 GHz. They are also similar to the frequencies of the two transitions found in the DBB host. ODMR signals were observed at the same frequencies when vibronic bands having energies higher than 20 903 cm^{-1} were monitored. At the 20 903-cm^{-1} band, however, two new signals were observed at 0.72 and 2.59 GHz, indicating that the 20 903-cm^{-1} band originates from a different species. The intensity of the 20 903-cm^{-1} band is not reduced by extensive purification of indazole. Furthermore, this band was not observed in the DBB host and in the BAC neat crystal. Thus the possibility that this band is due to an impurity seems to be remote. The relative intensity of this band with respect to the 23 590-cm^{-1} band does not change with the irradiation time. Therefore, this species is not photochemically induced. These observations strongly suggest that the 20 903-cm^{-1} band is due to indazole itself. It was thought that this species might be 2H, which was formed in the favorable environment of the BAC host. In order to confirm this possibility, we have compared the observed properties with those of 1-methylindazole and 2-methylindazole. Since methyl substitution is not expected to affect the triplet-state energy and the zfs greatly, 2H and 2-methylindazole should have similar triplet state energies and zfs.

The methyl-substituted indazoles did not dissolve into the BAC host, and so they were studied in the DBB host. The triplet energy obtained from the 0–0 band and the zero-field ODMR transition frequencies are 23 167 cm^{-1}, 1.89 GHz, and 2.25 GHz, respectively, for 1-methylindazole. The corresponding values for 2-methylindazole are 20 580 cm^{-1}, 0.64 GHz, and 2.56 GHz. The former values are similar to those of the 23 590-cm^{-1} band of indazole in BAC, while the latter values are similar to those of the 20 903-cm^{-1} band of imidazole in BAC. Furthermore, the triplet energies and the zero-field splittings of methylindazoles in ethanol–methanol mixtures are also similar to those of the two components of indazole in BAC as shown in Table I. On the basis of these observations we assign the 23 590-cm^{-1} band to 1H and the 20 903-cm^{-1} band to 2H.

The zero-field parameters of 1H and 2H are determined from the ODMR results by the spin Hamiltonian

$$\mathcal{H} = D(S_z^2 - {}^1/_3S^2) + E(S_x^2 - S_y^2) = -XS_x^2 - YS_y^2 - ZS_z^2 \quad (1)$$

where $X = (D/3) - E$, $Y = (D/3) + E$, and $Z = -(3/2)D$. Here we take the two in-plane spin axes as X and Y axes. The Z axis

(21) V. Auwers and M. Duisberg, *Ber.*, **53**, 1179 (1920).
(22) P. Schad, *Ber.*, *26*, 218 (1893).
(23) D. S. Tinti, M. A. El-Sayed, A. H. Maki, and C. B. Harris, *Chem. Phys. Lett.*, **3**, 343 (1969).
(24) J. Schmidt and J. H. van der Waals, *Chem. Phys. Lett.*, **3**, 546 (1969).
(25) J. Schmidt, W. S. Veeman, and J. H. van der Waals, *Chem. Phys. Lett.*, **4**, 341 (1969).
(26) D. A. Antheunis, J. Schmidt, and J. H. van der Waals, *Chem. Phys. Lett.*, **6**, 255 (1970).
(27) D. A. Antheunis, J. Schmidt, and J. H. van der Waals, *Mol. Phys.*, **22**, 1 (1971).
(28) S. Nagaoka and N. Hirota, *J. Chem. Phys.*, **74**, 1637 (1981).
(29) G. A. Sim, J. M. Robertson, and T. H. Goodwin, *Acta Crystallogr.*, **8**, 157 (1955).
(30) E. T. Harrigan and N. Hirota, *J. Am. Chem. Soc.*, **97**, 6647 (1975).

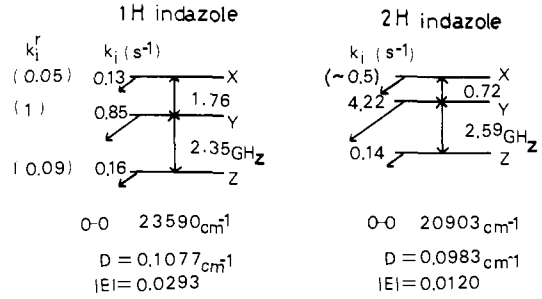

Figure 3. Summary of the zero-field sublevel schemes and the decay rate constants of 1*H*-indazole and 2*H*-indazole in BAC host; k_i and k_i^r are the total and the relative radiative decay rate constants, respectively. k_x of 2*H*-indazole was estimated from the decay rate at 77 K.

is taken perpendicular to the molecular plane. The T_z sublevel is considered to be the bottom sublevel as in the cases of other aromatic molecules. The top sublevel is taken as the X sublevel. The directions of the *X* and *Y* axes are determined by the ratio of the radiative decay rate constants and the angular dependence of hfs. The angular dependence of the EPR signals given in a later section unambiguously shows that $|T_x - T_y| < |T_y - T_z|$ or $D > 3|E|$. This is in contrast to the cases of indole and purine with $D < 3|E|$.[30] Both *D* and $|E|$ of 2H are considerably smaller than those of 1H (Table I).

B. Decay Properties of Two Tautomers. The relatively long lifetimes of 1H and 2H indicate that the T_1 states are $\pi\pi^*$ in character. The total decay rate constants (k_i) and the relative radiative decay rate constants (k_i^r) of the triplet sublevels were determined by the MIDP experiments. In 1H two MIDP signals corresponding to the X $\leftrightarrow$ Y and Y $\leftrightarrow$ Z transitions were observed and the total and the relative radiative decay rate constants of three sublevels were obtained. On the other hand, in 2H only one MIDP signal corresponding to the Y $\leftrightarrow$ Z transition was obtained. Assuming that the Z sublevel is not strongly radiative as in the usual $^3\pi\pi^*$ aromatics it can be concluded that $k_y^r \gg k_z^r$. We have attempted to determine the decay rate constant of the X sublevel of 2H from the fast passage experiment[31,32] for the X $\leftrightarrow$ Y transition, but the signal only showed the decay due to the Y sublevel. This result, however, indicates that $k_y^r \gg k_x^r$ for 2H. The results on the decay rate constants are summarized in Figure 3.

In spite of low molecular symmetries the decay rate constants are remarkably sublevel dependent. In both 1H and 2H the total and the relative radiative decay rate constants of the Y sublevels are by far the largest. The Y sublevel rate constants (k_y) of 1H and 2H are about 3 and 15 times larger than that of indole,[33] respectively. These increases of the decay rate constants are presumably due to the addition of the nitrogen atom to the indole structure, which brings in a low-energy $^1n\pi^*$ state. If we assume that the mixing with the $^1n\pi^*$ state is important in both radiative and nonradiative decay mechanisms, the one-center integral at the nitrogen atom becomes most important in the spin–orbit coupling matrix element relevant in these decays. Then the Y sublevel dominance in the radiative and nonradiative decays is expected when the *Y* axis is nearly perpendicular to the direction of the nitrogen nonbonding orbital. When the one-center integral at the nitrogen atom is dominant in the relevant spin–orbit coupling matrix element for the radiative decay, the ratio of k_y^r to k_x^r is given by[34]

$$k_y^r/k_x^r = \cos^2\alpha/\sin^2\alpha \qquad (2)$$

where α is the angle between the *X* axis and the direction of the nitrogen lone-pair orbital. For 1H, $k_x^r/k_y^r = 0.05$ gives $\alpha = 13°$. Therefore, the *X* axis is nearly along the long axis of the molecule. Similarly the *X* axis of 2H is concluded to be nearly along the short axis of the molecule from $k_y^r \gg k_x^r$.

Table II. Triplet Spin Densities Normalized to 1[a]

	1*H*-indazole		2*H*-indazole	
ρ	exptl	UHF	exptl	UHF
1		0.065		0.19
2		0.015		0.10
3		0.085	$\leqslant\sim$0.12	0.065
4	0.25 (0.19)	0.37	0.27 (0.26)	0.27
5	0.31	0.25	$\leqslant\sim$0.12	−0.079
6		−0.075	0.27	0.24
7	0.19 (0.25)	0.31	0.26 (0.27)	0.31
8		0.013		−0.08
9		−0.03		−0.02

[a] Position parameters of 1*H*-indazole for UHF calculation are taken from ref 16. Those of 2*H*-indazole are the same as those of pyrazole.[41]

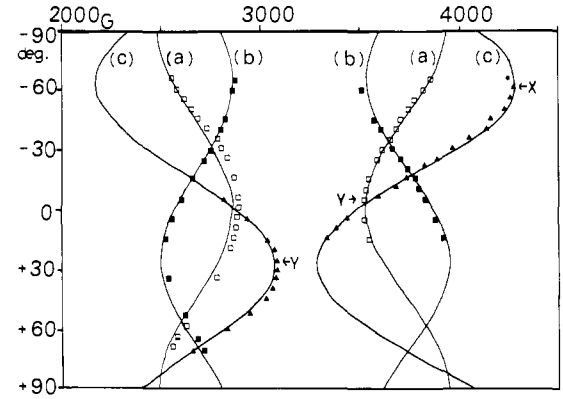

Figure 4. Angular dependence of the EPR signals of indazole in BAC at 4.2 K. Crystals were oriented so that $\vec{H}$ rotates in the molecular plane of a BAC molecule. (a) □ and (b) ■ indicate the angular dependence of the signals of 2*H*-indazole. (c) ▲ indicates that of 1*H*-indazole. Lines represent the angular dependence calculated with the spin Hamiltonian (eq 3).

The decay rate constant of the Y sublevel of 2H is about 5 times larger than that of 1H. Though quantitative comparison is difficult, the relatively weak phosphorescence intensity of 2H in spite of stronger intensity of the EPR signals seems to indicate that the larger decay rate constant of 2H is mainly due to the increase of the nonradiative decay rate constant. This increase of the nonradiative decay rate constant is expected from the Robinson–Frosch energy gap law,[35,36] because $E(T_1) - E(S_0)$ of 2H is about 2700 cm^{-1} less than that of 1H. Furthermore, the result of the UHF calculation shows that the spin density on the nitrogen atom containing lone pair electrons is larger for 2H (Table II). This would increase the spin–orbit coupling matrix element for 2H leading to an increased decay rate constant.

C. Angular Dependence of the EPR Signals and the Orientations of Indazole in the BAC Crystal. In Figure 4 we show the angular dependence of the EPR signals of 1H and 2H obtained at 4.2 K with the applied field rotating within the molecular plane of one of the molecules in the unit cell of the BAC crystal. The angular dependence of the EPR signals is given by solving the spin Hamiltonian

$$\mathcal{H} = g\beta\vec{H}\cdot\vec{S} + DS_z^2 + E(S_x^2 - S_y^2) \qquad (3)$$

Curves a, b, and c in Figure 4 are those predicted by using eq 3 and $g = 2$ and the *D* and *E* values determined from the ODMR experiments under the assumption $D > 3|E|$. Curves a and b are for 2H and (c) is for 1H. The agreements between the experimental points and the predicted curves are not perfect, but close enough to conclude that these signals are due to 1H and 2H,

(31) C. J. Winscom and A. H. Maki, *Chem. Phys. Lett.*, **12**, 264 (1971).
(32) A. L. Shain and M. Sharnoff, *Chem. Phys. Lett.*, **16**, 503 (1972).
(33) M. Noda, S. Nagaoka, and N. Hirota, to be submitted for publication.
(34) M. S. Groot, I. A. M. Hesselmann, H. F. Rienders, and J. H. van der Waals, *Mol. Phys.*, **29**, 37 (1975).
(35) G. W. Robinson and R. P. Frosch, *J. Chem. Phys.*, **37**, 1962 (1962).
(36) W. Siebrand, *J. Chem. Phys.*, **47**, 2411 (1967).

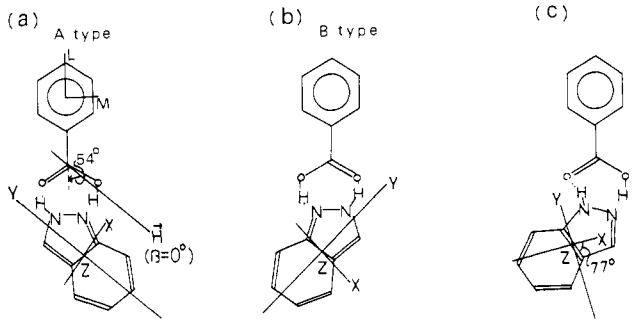

Figure 5. Directions of the principal axes of the zfs tensor, and the possible orientations of 2*H*- and 1*H*-indazole in BAC. The dotted lines indicate possible hydrogen bondings: (a) 2*H*-indazole gives the angular dependence of Figure 4a; (b) 2*H*-indazole gives the angular dependence of Figure 4b; (c) 1*H*-indazole gives the angular dependence of Figure 4c.

respectively. We mounted the crystal by assuming that the substituted indazole and the BAC that it replaces are coplanar, but a slight deviation from coplanarity may be the cause of the disagreement between the observed and calculated angular dependences. Curve a coincides with curve b by parallel displacement of 110° ± 3°. From these data we determine the orientations of indazole in BAC.

We measure the angle (β) of the direction of the applied field from the position at which the applied field is parallel to the Y direction of 2H, giving curve a (A-type indazole). At this position the direction of the applied field is rotated by 54° from the direction of the long axis (L axis) of BAC as shown in Figure 5. From the analysis of the hfs discussed in the following section we can conclude that the Y direction of 2H is 10° away from the N–H direction. Hence the orientation of the A-type indazole is given as shown by Figure 5a. The 2H giving the b curve (B-type indazole) is obtained by rotating the A-type indazole by 180° with respect to the L axis of BAC. The orientation of the B-type indazole is then given by Figure 5b. The b curve should be obtained by parallel displacement of the a curve by 108°. The observed value of 110° is in good agreement with the prediction within the experimental error. It is known that BAC molecules in the crystal assume two orientations[37,38] with different directions of the C=O group with respect to the crystal axes as shown in Figure 3 of ref 28. By forming hydrogen bonds with BAC in the two orientations 2H can have the two orientations as shown in Figure 5a, b.

The Y stationary points of 1H are 30° away from those of the A-type 2H. The analysis of the decay rate constants and the hfs indicate that the Y direction of 1H is nearly along the short axis of the molecule. The orientation of 1H in the crystal is then approximately as shown in Figure 5c. Evidence for a second orientation of 1H in the crystal was not found in the EPR spectra. The EPR signals of 2H were found to be stronger than those of 1H indicating that 2H is the major component in the T_1 state in the BAC host.

D. Hyperfine Splittings and Spin Distributions. Well resolved hfs were observed in the spectra of 2H at many directions of the applied field. On the other hand, 1H gave resolved hfs only in the neighborhood of the X stationary point. The hfs are analyzed by adding the terms representing the hyperfine interaction ($\sum_j \vec{S}\cdot A_j \cdot \vec{I}_j$) and the nuclear Zeeman term ($\sum_j \beta_n \vec{H}\cdot g_n \cdot \vec{I}_j$) to eq 3. We first discuss the hfs of 2H.

The most notable observation about the hfs of 2H is that the hfs of the high- and low-field signals are different. In Figure 6a the spectra taken with $H \| Y$ are shown. The high-field signal consists of six lines while the low-field signal shows seven components. This anomaly arises from the presence of forbidden lines due to the fact that the hyperfine coupling energies and the nuclear

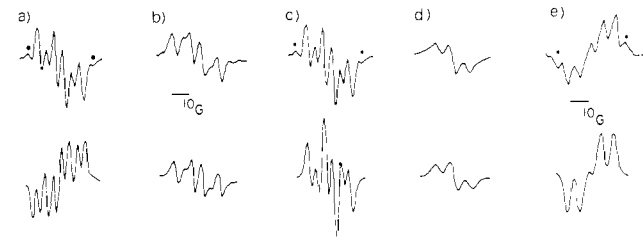

Figure 6. Hyperfine structure in the EPR spectra of indazoles in BAC at 4.2 K: (a) 2*H*-indazole, $H \| Y$ ($\beta = 0°$), high field (upper) and low field (lower); (b) 2*H*-indazole, $\beta = +10°$; observed (upper) and simulated (lower) spectra; (c) 2*H*-indazole, $\beta = 0°$; (d) 2*H*-indazole, $\beta = -10°$; (e) 1*H*-indazole, $H \| X$. In (a), (c), and (e) the first small peaks indicated by ▼ are probably due to forbidden transitions.

Zeeman energies of the protons are comparable at low field as similar behavior is found in the EPR spectra of the radical pairs of irradiated potassium deuterated fumarate[39] and the triplet state of *p*-xylene.[40] When $g_n\beta_n H \simeq -A$, the low-field signals are strongly affected by the forbidden lines. Therefore, we analyze the hfs using the high-field spectra.

The hfs observed at the Y stationary point can be simulated with three coupling constants: 9.6, 9.3, and 4.2 G. The spectra observed at other directions were simulated by changing the values of these coupling constants. Examples of the observed and simultated spectra are shown in Figure 6b–d. Using the coupling constants determined from the simulations, we obtain the angular dependence of the hfs shown in Figure 7. When the applied field is rotated in the molecular plane, the hfs of a proton in the high-field transition at a direction where the applied field makes an angle θ with the direction perpendicular to the C–H direction is given by[40]

$$\Delta h(\beta) = [(\rho A_{\hat{x}\hat{x}} \cos^2\theta - \rho A_{\hat{y}\hat{y}} \sin^2\theta - g_n\beta_n H)^2 + (\rho_2/4) \times (A_{\hat{x}\hat{x}} - A_{\hat{y}\hat{y}})^2 \sin^2 2\theta]^{1/2} - g_n\beta_n H \quad (4)$$

Here $A_{\hat{x}\hat{x}} = -36.5$ G, $A_{\hat{y}\hat{y}} = -11.5$ G, and $A_{\hat{z}\hat{z}} = -23.6$ G[40,42] are the principal values of the hyperfine tensor of a proton attached to an aromatic carbon. ($\hat{x}$ and $\hat{y}$ are perpendicular and parallel to the C–H direction, respectively. $\hat{z}$ is perpendicular to the molecular plane).

From Figure 7, we note that two splittings (Δh_1 and Δh_2) become the largest with $\beta = 10°$. At this direction the applied field must be parallel to the $\hat{x}$ direction of the hyperfine tensor of the two protons. Since the Y direction ($\beta = 0°$) is nearly along the long axis of the molecule, these observations unambiguously show that two hfs are due to the protons attached to carbons 4 and 7. The other splitting Δh_3 shows a minimum at $\beta = -20°$. At this direction $\vec{H}$ becomes parallel to C–H at position 6, indicating that the proton attached to the carbon 6 is responsible for the remaining splitting. Referring to Figure 7, θ is related to β by $\theta = \beta - \beta_1$ for the protons at the 4 and 7 positions and $\theta = \beta_1 - \beta + 60°$ for the proton at position 6. (β_1 is the angle between the Y axis of zfs and the $\tilde{Y}$ axis, which is the long axis of the molecule.) We have attempted to fit the observed angular dependences. As Figure 7 shows, $\rho_{4,7} = 0.26$, $\rho_{4,7} = 0.27$, and $\beta_1 = 10°$ produces a satisfactory agreement between the observed and the calculated angular dependences for Δh_1 and Δh_2. The best fit to Δh_3 was obtained with $\rho_6 = 0.27$. We were not able to resolve hfs due to other protons. The simulations were normally made with the line width of ~4.5 G, and the hfs due to other protons must be hidden within this width. This means that ρ_3 and ρ_5 must be smaller than ~0.12.

We have made a π-electron UHF (unrestricted Hartree–Fock method) calculation of the two tautomers in order to see whether the experimentally determined spin densities are consistent with

(37) S. Hayashi and J. Umemura, *J. Chem. Phys.*, **60**, 2630 (1974).
(38) J. Umemura and S. Hayashi, *Bull. Inst. Chem. Res. Kyoto Univ.*, **53**, 180 (1975).
(39) K. Minakata and M. Iwasaki, *Mol. Phys.*, **23**, 1115 (1972).
(40) Ph. J. Vergragt, J. A. Kooter, and J. H. van der Waals, *Mol. Phys.*, **33**, 1523 (1977).
(41) H. W. W. Ehrlich, *Acta Crystallogr.*, **13**, 946 (1960).
(42) N. Hirota, C. A. Hutchison, and P. Palmer, *J. Chem. Phys.*, **40**, 3717 (1964).

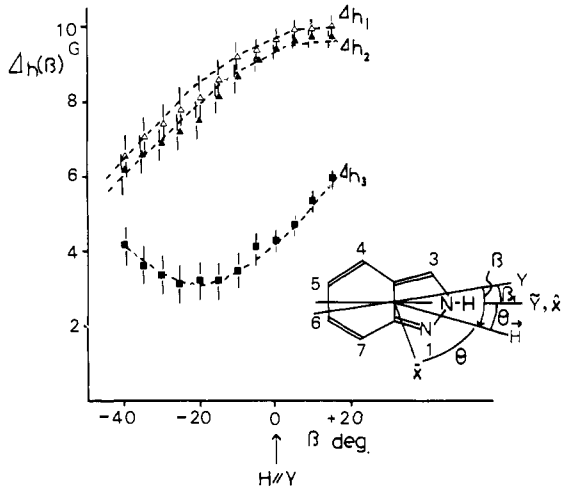

Figure 7. Angular dependence of the hyperfine splitting constants $\Delta h(\beta)$ (in gauss) for the high-field resonance lines (Figure 4a) of 2*H*-indazole. The bars indicate the errors in the experimentally estimated splitting constants. The line for Δh_1 is calculated by eq 4 with the values $\rho = 0.27$, $\beta_1 = 10°$, and $\theta = \beta - \beta_1$. The line for Δh_2 is calculated with $\rho = 0.26$, $\beta_1 = 10°$, and $\theta = \beta - \beta_1$. The line for Δh_3 is calculated with $\rho = 0.27$, $\beta_1 = 10°$, andd $\theta = \beta_1 - \beta + 60°$. Y and $\hat{x}$ indicate the directions of the Y axis of the zf tensor and the $\hat{x}$ axis of the hyperfine tensor, respectively. $\vec{H}$ represents the direction of the applied field. $\hat{Y}$ is the long axis of the molecule. The angle β_1 between the Y and $\hat{Y}$ is obtained from the experiment. The angle θ between the hyperfine axis $\hat{x}$ and the direction of $\vec{H}$ is equal to $\beta - \beta_1$ for $C_{4,7}$–H and $\beta_1 - \beta + 60°$ for the C_6–H.

those obtained by the calculation. The procedure used in the calculation is the same as that described previously.[28] In substituted benzenes such UHF calculations provide spin densities which are in good agreement with the experimental ones. The results are given in Table II. The calculation for 2H predicts large values for ρ_4, ρ_6, and ρ_7, as found experimentally. The calculated ρ_4, ρ_6, and ρ_7 are indeed close to the experimental values.

In the neighborhood of the X stationary point 1H shows partially resolved hfs which can be simulated with three splittings of 8.7, 6.8, and 4.4 G as shown in Figure 6e. Two outside small peaks were not considered because they are probably due to forbidden transitions. Unfortunately hfs were not observed in other directions and we cannot make an unambiguous assignment of the hfs. However, the X axis is nearly along the long axis of the molecule and the two large splittings are likely due to the protons at the 4 and 7 positions. From the analysis of the radiative decay rate constants, it was estimated that the X direction makes an angle of 77° with the directions of the C–H bonds at positions 4 and 7. With this angle, ρ_4 and ρ_7 are estimated to be 0.25 and 0.19, respectively, or vice versa. The 4.4-G splitting cannot be assigned experimentally, but the result of the UHF calculation indicates that the positions of large spin densities are 4, 5, and 7. Thus, this splitting may be assigned to the proton at 5. ρ_5 is estimated to be 0.31 by using eq 4. The values of ρ_4 and ρ_7 estimated experimentally are considerably smaller than the calculated values, though the experimental values have large uncertainties. The calculation shows that the main difference in the spin distribution between 1H and 2H is in ρ_5 and ρ_6. In 1H ρ_5 is large, while ρ_6 is large in 2H.

E. Hyperfine Anomalies of the Low-Field EPR Signals of 2H. As mentioned briefly in the previous section, the hfs of the low-field EPR signals of 2H are quite different from those of the high field ones because of the presence of the additional lines due to forbidden transitions. In Figure 8 the angular dependence of the low-field spectra in the neighborhood of the Y stationary point is given. It is seen in Figure 8 that the lines indicated by ▲ and O gradually change in intensity as the angle changes from $\beta = +20°$ to 0°. These changes are believed to be caused by the changes from the forbidden lines to the allowed ones and vice versa as the direction of the applied field rotates away from the principal direction of the C_6–H hyperfine tensor. This is because the

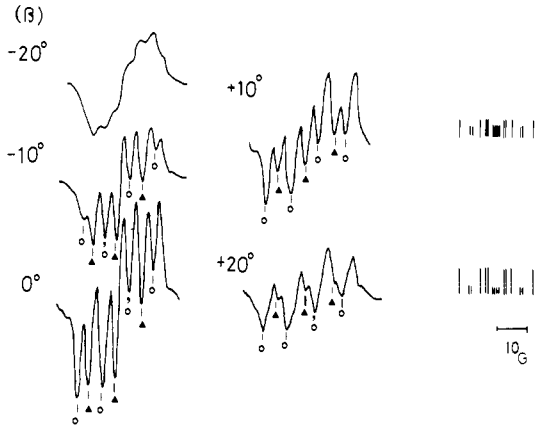

Figure 8. Angular dependence of the low-field hyperfine spectra of 2*H*-indazole in BAC (Figure 4a). The angles shown are the same as those in Figure 4. Two stick diagrams are explanatory of the EPR spectra at +10° and +20°, respectively.

hyperfine energy is comparable to the Zeeman energy for this proton. We have attempted to explain the observed changes following the treatment given by Minakata and Iwasaki[39] using $\rho_{4,7} = 0.27$, 0.26, and $\rho_6 = 0.27$. The predicted positions and intensities of the hyperfine lines are given by stick diagrams in Figure 8. The characteristic features of the low-field hyperfine pattern are qualitatively explained, though quantitative agreement is not perfect. It is seen that the forbidden lines gain intensities with the decrease of β.

Summary and Concluding Remarks

The phosphorescence spectrum of indazole in the BAC crystal consists of two spectra with the 0–0 bands at 23 590 and 20903 cm^{-1}, respectively. From the comparison with the properties of methylindazoles it is concluded that these two spectra arise from two tautomers (1H and 2H) of indazole in the T_1 states. The zfs and the spin distributions and the decay properties of the T_1 states of both tautomers are determined by the EPR and ODMR experiments. The decay and magnetic properties of the two tautomers are somewhat different, though the phosphorescence decay takes place predominantly from the Y sublevel in both tautomers. From the angular dependence of the EPR signals the orientations of the two tautomers in the BAC crystal are determined. Indazole is considered to be hydrogen bonded with BAC.

Previous investigations seem to indicate that indazole in the ground state does not exsist in the 2H form. Thus it is likely that 2H is formed from 1H in the excited state. It is seen from Figure 5 that double proton switching along the hydrogen bonds with BAC converts 1H into 2H. Hence it is speculated that proton transfer in the excited singlet state of 1H produces 2H. Preliminary results on the phosphorescence excitation spectra seem to suppport this view. It should be noted that the excited state tautomerism in the nitrogen heterocyclics caused by proton transfer is known in the case of 7-azaindole.[43-47] Further investigations on the mechanism of the tautomerization and proton transfer in the excited state of indazole are currently in progress.

Acknowledgment. We with to thank S. Nagaoka for his help in conducting this work.

Registry No. 1*H*-Indazole, 271-44-3; 2*H*-indazole, 271-42-1; benzoic acid, 65-85-0.

(43) C. A. Taylor, M. A. El-Bayoumi, and M. Kasha, *Proc. Natl. Acad. Sci. U.S.A.* **63**, 253 (1969).
(44) K. C. Ingham and M. A. El-Bayoumi, *J. Am. Chem. Soc.*, **96**, 1674 (1974).
(45) M. A. El-Bayoumi, P. Avouris, and W. R. Ware, *J. Chem. Phys.*, **62** 2499 (1975).
(46) W. M. Hertherington, R. H. Micheels, and K. B. Eisenthal, *Chem. Phys. Lett.*, **66**, 230 (1979).
(47) J. Waluk, H. Bulska, B. Pakula, and J. Sepiol. *J. Lumin.*, **24/25**, 519 (1981).